バイオサイエンス研究科　博士論文要旨

所属 （主指導教員）	細胞構造学講座　(塩坂　貞夫　教授)		
氏名	中村　雪子	提出	平成　17 年 12 月 26 日
題目	Role of neuropsin in formation and maturation of Schaffer-collateral L1cam-immunoreactive synaptic boutons (Schaffer-collateral 回路における L1cam 免疫陽性 synaptic bouton の形成と成熟に関するニューロプシンの役割について)		

要旨

I report that secretory protease neuropsin (NP) is involved in the synaptogenesis/maturation of orphan and small synaptic boutons in the Schaffer-collateral pathway. Synaptogenesis occurs not only in development but also in adult stage. Recently, it is suggested that the synaptogenesis in adult stage is important to acquisition of memory. In hippocampus, many orphan boutons which have synaptic vesicle but not contact with postsynaptic specialization are exist, and the structure is considered as first stage of synaptogenesis. In synaptogenesis, orphan bouton contacts with spine and makes small immature synaptic formation, then the synapse is enlarged and matured following insertion of AMPA receptor and other molecules. The small synapse is more flexible and is considered as important to acquisition of memory. But it has been not known what molecules lead to make the synaptic contact and how to change the immature synapse to mature synapses depending on neural stimulation.

I focused on cell adhesion molecule L1 which is known as important molecule for construction of neural circuit in development stage. Our laboratory showed that L1 exists abundantly in the brain not only in development stage but also in adult stage. In addition, Luiti et al. showed that L1 is also important to induction of long-term potentiation which is an index of learning and memory. In this study, I appeared that most of non-synaptic orphan boutons and a number of immature small synaptic boutons expressed the cell adhesion molecule L1 in presynaptic Schaffer-collateral terminals, whereas mature large boutons on mushroom spines were devoid of L1.

By neural stimulation, L1 is cleaved via NP which is also important molecule to induction of long-term potentiation. Therefore, I expected that these two molecules are contributed to changing synaptic efficacy. In this study, I examined the effect of neuropsin to L1 using neuropsin deficient mice. In NP-deficient mice, the number of L1-immunoreactive orphan and synaptic boutons was markedly higher than in wild-type mice, while there were far fewer mature large boutons. L1-immunoreactive boutons were hypertrophied in the mutant mice. When a recombinant active NP was microinjected into the mutant hippocampus, the number of immunoreactive synaptic boutons reverted to wild-type levels after one day. These results strongly suggest that enzymatically active NP allows a maturational change of L1-immunoreactive small boutons, both orphan and synaptic, and this step may be important in structure-based synaptic plasticity.

Role of neuropsin in formation and maturation of Schaffer-collateral L1cam-immunoreactive synaptic boutons

(Schaffer-collateral 回路における L1cam 免疫陽性 synaptic bouton の形成と成熟に関するニューロプシンの役割について)

中村　雪子

奈良先端科学技術大学院大学

バイオサイエンス研究科　細胞構造学講座

（塩坂　貞夫教授）

平成 17 年　12 月 26 日　提出

Contents

Chapter 3 Result

Acknowledgments

Introduction

The dynamic regulation of synaptic strength by neural activity, i.e. rapid quantitative and qualitative changes in synapses, is fundamental to aspects of neural plasticity such as learning and memory. A number of studies have concentrated on the glutamatergic receptor function and signal transduction (Collingridge and Bliss, 1995). It has recently been suggested that an activity-dependent modification of extracellular molecules occurs in the vicinity of asymmetrical synapses modulates synaptic morphology (Benson et al., 2000; Shiosaka and Yoshida, 2000). Spines forming asymmetric synapses are morphologically divided into at least two types, thin and mushroom; the former have a much smaller head than the latter (Fiala and Harris, 1999). Matsuzaki et al. (2004) have shown, using two-photon photolysis of caged glutamate at single spines, that glutamate release induces a rapid and selective enlargement of the stimulated spine. Spine head size is clearly related to the induction of long-term potentiation (LTP), which is transient in large mushroom spines but persistent in small spines. The enlargement of spines is associated with the accumulation of AMPA (α amino-3-hydroxy-5-methyl-4-isoxazole propionic acid) receptors, implying potentiation of synaptic efficacy. Takumi et al. (1999) revealed by immunoelectron microscopy that

the postsynaptic density (PSD) of small synapses lacked AMPA receptors, and thus are expected to be 'silent synapses'. Matsuzaki et al. (2004) also suggested that small spines are preferential sites for the induction of LTP, whereas larger spines represent physical traces of long-term memory. Collectively, small synapses in contact with small spines with small PSDs are considered plastic structures ready for the acquisition and consolidation of memory. However, the molecules which participate in these synaptic structural changes and the mechanisms involved in synaptogenesis/maturation have not yet been identified.

The secretory protease neuropsin (NP) is associated with activity-dependent neural plasticity, i.e., LTP and kindling epileptogenesis (Okabe et al., 1996; Momota et al., 1998; Komai et al., 2000). When recombinant active NP (actNP) protein was bath-applied to hippocampal slices, LTP was facilitated, whereas application of an anti-NP antibody that neutralizes the protease activity resulted in a deterioration of LTP (Momota et al., 1998; Komai et al., 2000). In the NP-deficient mice, the number of non-synaptic orphan boutons was significantly increased, whereas asymmetrical mature type synapses were decreased (Hirata et al., 2001). Matsumoto-Miyai et al. (2003) have recently shown that neural excitation triggers a transient activation of proNP (zymogen) to cleave full length cell adhesion molecule L1 ($L1_{200}$) into $L1_{180}$ (180-kDa fragment of

L1) in vitro. L1 has also been implicated in the generation of LTP, because application of L1 antibody or recombinant L1 fragment to hippocampus slices resulted in the decay of LTP (Luthi et al., 1994). These results showed that NP might participate in synaptic plasticity, including the regulation of synaptic transmission and synaptic structure, via cleavage of L1. However, the mechanism by which NP and L1 influence synaptic plasticity is not known. In the present study, I revealed that immature orphan and presynaptic small boutons containing L1 undergo a NP-dependent morphological change, becoming L1-negative asymmetrical boutons on the large mushroom-type spines. NP and L1 may therefore associate to regulate synaptogenesis/maturation of synaptic structures.

Materials and Methods

Animals

Production of NP-/- mice was described by Hirata et al. (2001). The mice were backcrossed six times with strain C57BL/6J. Mice were maintained according to guidelines of the Nara Institute of Science and Technology, and the study was approved by the institutional animal care and use committee.

Histology

Tissue preparation

Male NP+/+ and NP-/- (8-week-old) mice were deeply anesthetized with an intraperitoneal injection of 10% ethylcarbamate (10 µl/g body weight) and perfused through the ascending aorta with 50 ml saline and then 100 ml fixative (0.1 M phosphate-buffered saline (PBS), pH 7.4, 4% paraformaldehyde, 0.05% glutaraldehyde). Brains were removed and postfixed overnight in the same fixative at 4°C and coronal-sectioned with a Microslicer (Dosaka EM, Kyoto, Japan) at a thickness of 30 µm. Tissue preparations and observations were all performed at the same front-caudal brain level (Bregma -2.30 mm) of the mouse brain atlas of Franklin and Paxinos (1996).

Immunohistochemistry

Light microscopy

The immunohistochemistry of L1 was as described previously (Munakata et al., 2003). Briefly, the tissue sections were incubated in ethanol (50% 10 min, 70% 10 min, 50% 10 min), following by washing three times with PBS for 10 min. These sections were pre-incubated in PBS containing 5% bovine serum albumin (BSA) (Sigma, St. Louis, MO) for 1 hour prior to the start of immunohistochemistry. The sections were incubated in anti-C-terminal L1 antiserum (Santa Cruz Biotechnology Inc., Santa Cruz, CA; 1:200) in two over night. For detection of anti-L1 antibody, biotinylated anti-goat immunoglobulin G (IgG) secondary antibody was used (Vector Laboratories, Burlingame, CA; 1:1000). For inactivation of endogenous peroxidase, These sections were incubated in PBS containing 1% H_2O_2 and 30% methanol, followed by washing three times with PBS for 10 min. Bound antibody was detected by staining for 2 hours with the ABC Vectastain kit (Vector Laboratories, Burlingame, CA) and then for 5 min with 0.05% 3,3'-diaminobenzidine tetrahydroxychloride (DAB) in 50mM Tris-HCl, pH 7.5, containing 0.01% H_2O_2. The sections were observed under a Zeiss Axioplan 2 microscope, and images of each section were captured with a C4742-95 digital camera

(Hamamatsu Photonics, Hamamatsu, Japan) and analyzed with Win Roof software (Mitani Co., Fukui, Japan).

Pre-embedding immunohistochemistry and quantitative electron microscopy

Sections for EM were postfixed with 1% OsO_4 in 0.1 M phosphate buffer (pH 7.4) for 1 hour at 4 °C, and dehydrated in a series of solutions (50% ethanol, 70% ethanol containing saturated uranyl acetate, 80% ethanol, 90% ethanol, 99% ethanol and 100% ethanol) in and propylene oxide. The sections were mounted with Epon 812 on a siliconized glass slide. After light microscopic observation, equivalent hippocampal regions of NP+/+ and NP-/- mice were cut out and sectioned with a Reinhardt ultramicrotome (Heidelberg, Germany) at a thickness of 80 nm, following by putting on the section to single slot Cu mesh. The ultrathin sections were stained with lead citrate and observed using a Hitachi H-7100 EM (Tokyo, Japan), and images were acquired using a Polaroid film scanner (Tokyo, Japan). The number of L1-immunoreactive (L1ir) and L1ir-negative boutons was counted in a fixed area (13.0 × 73.2 μm). Three consecutive sections were observed to determine whether boutons were orphan or synaptic for statistical analysis (Hirata et al., 2001).

Post-embedding immunohistochemistry

Small tissue blocks (300 μm) from the CA1 region of the hippocampus were incubated in water at 4 °C for 30 min and dehydrated in a series of ethanol solutions (30% ethanol at 4 °C for 30 min, 50%, 70%, 90%, 100% ethanol at -30 °C for 30 min each, and 0.5% uranyl acetate in 100% ethanol at -30 °C for 60 min). After washing by 100% ethanol at -30 °C for 60 min, these sections were incubated in ethanol containing 50%, 70%,100% Lowicryl K4M (Polysciences, Inc, Eppelheim, Germany) at -30 °C for 60 min each. Then these sections were embedded with 100% Lowicryl K4M at -30 °C in ultraviolet light (360 nm) for 48 h. Ultrathin sections (80 nm) were mounted on formvar-coated Ni grids and processed for immunogold histochemistry. Sections were immersed in 3% H_2O_2 for 3 min and incubated at room temperature for 10 min in 0.1% sodium borohydride and 50 mM glycine in 5 mM Tris-HCl containing 50 mM NaCl and 0.1% Triton X-100 (TBST), followed by incubation in 1% bovine serum albumin (BSA) in TBST, then for 12-16 hours in mixtures of goat antibodies to L1 diluted 1:100 in TBST containing 1% BSA. For detection of anti-L1 antibody, biotinylated anti-goat IgG secondary antibody was used (1:200). Then sections were placed in streptavidin-coupled 10-nm gold particle (EM.STP10; British BioCell International, Cardiff, UK) diluted 1:25 in TBST containing 1% BSA and polyethylene glycol (5

mg/ml) for 2 hours.

Statistical analysis

To count the number of synapses and orphan boutons and measuring spines and PSDs, 20 mice (10 NP+/+ and 10 NP-/-) were used. For counting synapses after injection of active NP into NP-/- mice, three animals were used and an investigator blind to the conditions performed all analyses. Mean numbers and size of L1ir and L1ir-negative boutons in NP+/+ and NP-/- mice were compared using unpaired two-tailed Student's T tests, and distribution analysis was performed using the Kolmogorov-Smirnov test.

In situ hybridization

In situ hybridization of L1 was described previously (Horinouchi et al., 2005). Briefly, 16-μm sections were fixed with 4% formaldehyde in 0.1 M phosphate buffer (pH 7.4) (PB), permeabilized with 10 μg/ml proteinase K in 50 mM Tris-HCl (pH 7.5) and 5 mM EDTA and acetylated in 0.1 M triethanolamine buffer containing 0.225% acetic anhydride. After dehydration, the sections were hybridized with 10^7 cpm/ml ^{35}S-labeled cRNA probe at 55℃ for 16 hours, washed, and then treated with RNaseA. After dehydration, the sections were dipped in Kodak NBT-2 emulsion (Rochester, NY) and

exposed for 1 month.

3D reconstruction of images from serial ultrathin sections

Entire synapses including spines and synaptic boutons were reconstructed from image stacks of 20 serial sections. Seventeen randomly selected synapses of L1ir and L1ir-negative boutons from NP-/- and NP+/+ mice were reconstructed. Digital images were aligned using IGL Trace software (developed by Dr. John C Fiala, Boston University, Boston, MA). Contours of axons, dendrites, PSDs and boutons were displayed three-dimensionally with GLView version 4.30 software (Bitmanagement Software GmbH, Germany).

Western blot analysis

Hippocampi were removed from 6 NP-/- and 6 NP+/+ (C57BL/6J) mouse brains. Each hippocampal organs were homogenized in ice-cold lysis buffer containing 20 mM Tris-HCl, 0.32 M sucrose, 1 mM EDTA, 1 mM sodium orthovanadate and protease inhibitor cocktail (Sigma, St. Louis, MO). The homogenates were centrifuged for 10 min at 900 × g to remove debris, nuclei, etc. The supernatant was treated with Triton X-100 at a final concentration of 1 %. Aliquots of the proteins were subjected to

SDS-PAGE and transferred onto PVDF membranes (Bio-Rad Laboratories, Hercules, CA). Membrane were pretreated with 5 % skim milk and 0.1 % Tween 20 in TBS (TBST), pH 7.4. The membrane was incubated with anti-C-terminal L1 mouse IgG (Santa Cruz Biotechnology Inc., Santa Cruz, CA; 1:2000) or anti-actin monoclonal IgG (Chemicon, Temecula, CA; 1:1000). After washing in TBST, the blots were incubated with alkaline phosphatase-conjugated rabbit anti-mouse IgG antibody. Immunoreactivity was detected with Immun-Star substrate (Bio-Rad Laboratories, Hercules, CA) on X-ray film according to the manufacturer's instructions. Band density was quantified with the Scion Image software (Scion, Frederick, MD).

Intracellular injections of Lucifer yellow

Mice were anesthetized with diethyl ether, and the brains were removed into modified Ringer solution (in mM: sucrose, 46.8; KCl, 0.5; NaH_2PO_4, 0.25; $NaHCO_3$, 5.2; glucose, 2.2; $MgSO_4$, 2; $CaCl_2$, 0.1) keeping it oxygenated (95% O_2/5% CO_2) for 5 min. The brain was cut on a vibratome (300 µm thickness), removed into oxygenated ACSF solution for 1-2 hours at 32 °C, and then transferred to cold 4% paraformaldehyde in 0.1 M PB for 45 min. Lucifer yellow was injected with an Eppendorf Microinjector 5242 (Hamburg, Germany) by applying negative current pulses (1.5 nA) for 10 min. Sections

with successfully filled neurons were transferred into cold 4% paraformaldehyde in 0.1 M PB, postfixed overnight, and then photographed under a Nikon Eclipse E600 microscope (Tokyo, Japan) to observe dendritic arbors and spines of CA1 pyramidal neurons.

Injection of active NP

Three 8-week-old NP-/- mice were anesthetized with 10% ethyl carbamate (1.25 mg/kg), placed in a stereotaxic apparatus, and injected with recombinant actNP using a 5-µl Hamilton (Reno, NV) syringe over 10 min. Stereotaxic coordinates relative to Bregma were 1.34 mm posterior and 1.20 mm lateral, and the tip of the infusion cannula (26 gauge) was located in the stratum radiatum of the CA1 field. The recombinant actNP was produced as described (Shimizu et al., 1998; Komai et al., 2000) and diluted with artificial cerebrospinal fluid (ACSF; in mM: NaCl, 127; KCl, 1.6; KH_2PO_4, 1.24; $MgSO_4$, 1.3; $CaCl_2$, 2.4; $NaHCO_3$, 26; glucose, 10). FITC-conjugated recombinant actNP was injected to observe the spread area of recombinant actNP over the hippocampal sublayers. The dose of recombinant actNP used in this study (0.8 µl, 3.0 mU/ml) was the optimum concentration leading to an increase of the Shaffer-collateral path-evoked fEPSP slope (unpublished data).

Electrophysiology

Male NP +/+, +/- and -/- mice were anaesthetized with urethane (1.25 g/kg; i.p.) and placed in a stereotaxic frame with the skull horizontal. Rectal temperature was maintained at 37 °C using a heated jacket pad (BWT-100, Bio Research Center, Nagoya, Japan). Extracellular field recording was carried out as previously described (Matsumoto-Miyai et al., 2003). A bipolar stainless-steel electrode (InterMedical Co., Tokyo, Japan) was used for stimulation in the Schaffer-collateral pathway (2.46 mm posterior and 2.30 mm lateral to bregma). Field excitatory postsynaptic potentials (fEPSPs) were recorded with a monopolar tungsten electrode (InterMedical Co.) placed in the stratum radiatum of the CA1 region (2.46 mm posterior and 2.0 mm lateral to bregma). After a stable response was reached, I-O curves were obtained over the range of 40 – 600 μA.

Results

L1 is localized to the presynaptic terminal boutons of the Schaffer-collateral pathway

L1ir was observed in axons which could be traced to CA3 pyramidal neurons (Fig. 1A, arrow, arrowheads) (Matsumoto-Miyai et al., 2003). In situ hybridization analysis demonstrated strong signals for L1 mRNA in the CA1-CA3 pyramidal neurons, implying that these cells produce L1 (Fig. 1B). L1ir was found in the axons of CA3 pyramidal neurons (Fig. 1C, D), axon bundles along the Schaffer-collateral pathway (Fig. 1E). In the Schaffer-collateral terminal area of the CA1 subfield, L1ir was detected in the axonal processes and in numerous protrusions from the axons (Fig. 1F, arrowheads). Electron microscopic (EM) observation of immunoreacted tissue sections using two different markers, diaminobenzidin or colloidal gold, revealed that L1ir was localized in the cytoplasm of small synapses (Fig. 1G,H,J,K) and orphan boutons (Fig. 1I,L), and associated with the presynaptic membrane of asymmetrical synapses that had thick PSDs (Fig. 1G,H,J,K, open arrowhead). When colloidal gold was used as a maker, clustering of gold particles on the presynaptic membrane was clearly visible on the presynaptic densities (Fig. 1J,K, open arrowheads). Thus, I conclude that L1 protein is

produced in the pyramidal cell body, transported by anterograde axonal transport through the axon, and accumulates in the presynaptic structure of terminal boutons.

All the positive presynaptic boutons had small heads containing a few synaptic vesicles, and were in contact with thin type spines having smaller PSDs as compared with L1ir-negative asymmetrical synapses (see Fig. 3C). Three-dimensional (3D) reconstruction of stacks of EM images acquired from consecutive ultrathin sections enabled us to see L1ir orphan and small synaptic boutons (Fig. 2). L1ir was distributed beneath the presynaptic membrane (Fig. 2Ab,Bb, red). Typical L1ir-negative axonal boutons had a large head contacting with mushroom-type large spines (Fig. 2Ac,Bc). Measurement of the spine head area and PSD length of all synapses present in a fixed square of a single-plane EM image showed that L1ir synapses were much smaller than L1ir-negative synapses (Fig. 3A-C, L1 versus L1neg). From their morphology, L1ir orphan or synaptic boutons were considered to be functionally immature or temporary structures for synaptogenesis/maturation of synapses (see Discussion).

Increased number of L1ir orphan and synaptic boutons in NP-/- mice

Since the activation of proNP zymogen and subsequent cleavage of L1 occur in the hippocampus in an activity-dependent manner (Matsumoto-Miyai et al., 2003), it was

hypothesized that NP converts immature (L1ir) into mature (L1ir-negative) synapses. Therefore, I explored whether NP-deficient (NP-/-) mice exhibit quantitative abnormalities in the immature (L1ir) and mature (L1ir-negative) boutons. Low-magnification electron micrographs clearly revealed larger numbers of L1ir orphan and synaptic boutons in the stratum radiatum of the CA1 subfield in the NP-/- mice than in the NP+/+ mice (Fig. 4A). L1ir deposits in the orphan and synaptic boutons were markedly denser in NP-/- than in NP+/+ mice (Fig. 4A). Western blot analysis showed that the marked increase in band density of L1ir in NP-/- than NP+/+ mouse hippocampus (Fig. 4B). These findings strongly suggested that L1ir accumulates in both structures in the NP-/- mice. To examine the difference in L1ir synaptic localization between NP-/- and NP+/+ mice, L1ir synaptic boutons were plotted on a montage of 25 low-magnification (× 6,000) electron micrographs covering all layers of the stratum radiatum and lacunosum moleculare. The density and topographic localization clearly differed between the two (Fig. 5A). L1ir synaptic boutons were more abundant, particularly in the proximal one-third of the stratum radiatum, in the NP-/- than in the NP+/+ mice (Fig. 5A). L1ir orphan boutons were much more numerous in the NP-/- mice, and deposits of immunoreactivity were much denser in these than in the NP+/+ mice (Fig. 4A, asterisks).

To confirm the results of visual inspection, I next analyzed NP-/- and NP+/+ hippocampus using quantitative immunoelectron microscopy (Fig. 5B, C). L1ir small and L1ir-negative large asymmetrical synapses were identified based on synaptic characteristics (i.e. the presence of synaptic vesicles, PSDs, an apposed synaptic membrane and a uniform synaptic cleft). The number and percentage of L1ir small synapses were significantly higher in the NP-/- compared to the NP+/+ mice (Fig. 5B; 9.27 ± 1.75% versus 4.87 ± 0.65%, $p < 0.05$). The difference was marked in the proximal one-third of the stratum radiatum (8.08 ± 1.19% versus 3.82 ± 0.85%, $p < 0.01$) (Fig. 5B; Table 1). The percentage of L1ir/total synapses was approximately two-fold higher in the mutant. On the other hand, the total number of asymmetrical synapses (L1ir and L1ir-negative) in the stratum radiatum was significantly lower in the proximal layer of the NP-/- hippocampus (Fig. 5C) (Hirata et al., 2001). Moreover, the majority of orphan boutons were L1ir and the number in the NP-deficient mice was also increased two-fold (Table 1). Intriguingly, the increase in L1ir orphan boutons was most apparent in the proximal one-third of the stratum radiatum (Fig. 5D, Table 1).

I examined the input-output (I-O) relationship of Schaffer collateral-CA1 synapses (Fig. 6). The I-O curves for fEPSP with 500 and 600 µA were different between NP-/- and NP+/+ mice. These data also suggest that the number of

synapses is lower in NP-/- mice than NP+/+ mice. These results, combined with our EM studies imply that the deficiency of NP induced an accumulation of L1ir orphan and small synaptic boutons, coincident with impairment of the formation of mature synapses.

Hypertrophied orphan and small synaptic boutons were often found in the NP-deficient mouse.

Since the quantitative measurements showed that L1ir orphan and synaptic boutons were markedly increased in the NP-/- mice, L1ir boutons were further assessed by measurement of the size of spine head area and PSD length in comparison with wild-type mice (Fig. 2Ba,b, NP-/- versus NP+/+; Fig. 3A-C). In the NP-/- mice, hypertrophy of orphan and synaptic boutons was apparent in the proximal one-third of the stratum radiatum, but not in the other layers (Fig. 3A, C). These results suggest that remodeling of synaptic structure occurs most frequently in this area, causing the hypertrophy and increase of L1ir presynaptic boutons in the mutant mice. Collectively, quantitative and qualitative examinations of the L1ir structures strongly support the idea that NP is involved in the conversion of L1ir orphan and synaptic boutons into L1ir-negative large synaptic boutons, particularly in the proximal part of the stratum

radiatum.

Injection of actNP rescued the quantitative but not qualitative abnormality in NP-deficient hippocampus

The findings in the mutant of a prominent accumulation and hypertrophy of L1ir orphan and synaptic boutons, and of a decrease in the number of L1ir-negative mature synapses, signify a conversion of L1ir orphan and synaptic boutons into mature synapses that lack L1ir. This issue was examined further by administering recombinant actNP into the NP-/- mouse hippocampus; if NP-dependent synaptic conversion occurs as in adults, supplying exogenous actNP to adult mutant mice might rescue the abnormality. Since NP is known to act extracellularly (Momota et al., 1998; Komai et al., 2000; Oka et al., 2002), recombinant actNP was microinjected into the stratum radiatum of the CA1 subfield in vivo. To assess the degree of spread of the actNP, an FITC-conjugated recombinant actNP was injected and found to spread over most of the stratum radiatum (Fig. 7A). After the potentiating effect of NP on extracellular postsynaptic potential (EPSP) was measured in vivo, the same mice were processed for immunoEM: i.e., one day after EPSP measurement, followed by quantitative immunoEM analysis of the proximal one-third of the stratum radiatum. When recombinant actNP was administered

by a single injection at a physiological dose, the number and percentage of L1ir synapses were significantly reduced to the levels seen in untreated wild-type mice (Fig. 7B), although the total synaptic number was similar to the group receiving ACSF injections (187.6 ± 10.5 for ACSF versus 198.7 ± 10.5 for activated NP). Thus, injected recombinant actNP mimics the function of endogenous actNP and can convert L1ir synapses into L1ir-negative mushroom spine synapses.

Light microscopic observation of postsynaptic neurons in NP-/- mice

The finding that synaptic number and morphology was abnormal in NP-/- mice suggested that there might be changes in the postsynaptic neurons in the mutants. Therefore, I examined the density of spines by microinjecting Lucifer yellow, a fluorescent dye, into pyramidal neurons of the CA1 subfield and by 3D observation using a two-photon microscope. However, there were no apparent differences number of spines in the dendrites between the two genotypes (Fig, 8A-C), nor in the morphology of dendritic arbors or the length of the apical dendrites (Fig. 8A). These observations were confirmed using the Golgi impregnation method, which showed no detectable difference in the density of spines between the two genotypes in the CA1 subfield (data not shown). However, the morphology of the spines appeared to be changed and

irregularly shaped spines (thin spines which can not be categorized into mushroom, thin, and stubby, e.g. branched spine) were increased in the NP-/- mice compared to the NP+/+ mice in the CA1 subfield (2.4 ± 04 versus 1.2 ± 0.3, $p < 0.05$). I therefore conclude that NP deficiency induced the abnormal morphology of the spines.

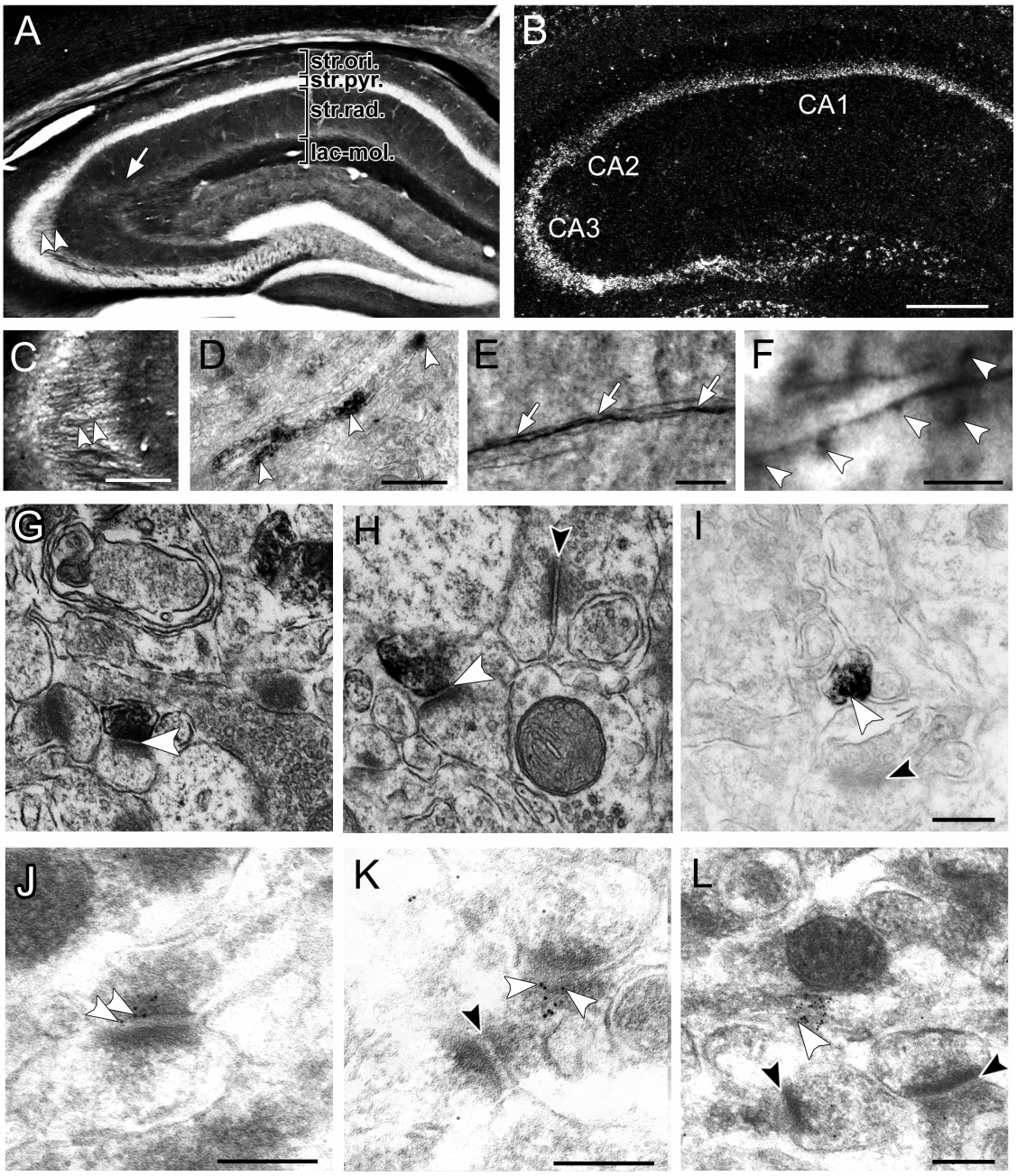

Figure 1. L1 localization to presynaptic terminals in the Schaffer-collateral pathway.

(A) Overview of staining by anti-L1 antibody with DAB in the hippocampus of adult mice. The arrowheads point to strongly stained black bundles from CA3 soma and immunoreactive fibers projected toward the stratum radiatum in the CA1 subfield (arrow). Stratum oriens (str. ori.), stratum pyramidale (str. pyr.), stratum radiatum (str.

rad.) and lacunosum-moleculare (lac-mol.) are indicated.
(B) Expression of L1 mRNA in hippocampus detected by in situ hybridization. Intense hybridization signals in the pyramidal layer, especially in CA3 pyramidal cells, appear as silver grains under dark-field illumination. Scale bar, 300 μm.
(C) Higher magnification of L1ir axon bundles from CA3 soma marked by arrowheads in (A). Scale bar, 100 μm.
(D) Immunoelectron microscopic analysis of regions marked by arrowheads in (A, C). L1ir is observed on and in axons (arrowheads). Scale bar, 1 μm.
(E) Higher magnification of L1ir fibers marked by arrow in (A). Some fasciculated axons show L1ir (arrows). Scale bar, 5 μm.
(F) Higher magnification of an L1ir axon in the CA1 stratum radiatum. Arrowheads indicate L1ir boutons on axons. Scale bar, 5 μm.
(G-I) Immunoelectron microscopic localization of L1 by pre-embedding staining in the CA1 stratum radiatum. L1ir is distributed in presynaptic sites of asymmetrical synapses (open arrowheads). L1ir was observed in orphan boutons containing a few vesicles (I). Closed arrowheads are L1ir-negative asymmetrical synapses. Scale bar, 300 nm.
(J-L) Immunogold labeling of L1ir in CA1 stratum radiatum. Gold particles (10 nm, indicated by open arrowheads) are associated with the presynaptic membrane, the presynapse interior (J, K), and orphan boutons (L). Closed arrowheads indicate L1ir-negative asymmetrical synapses. Scale bar, 300 nm.

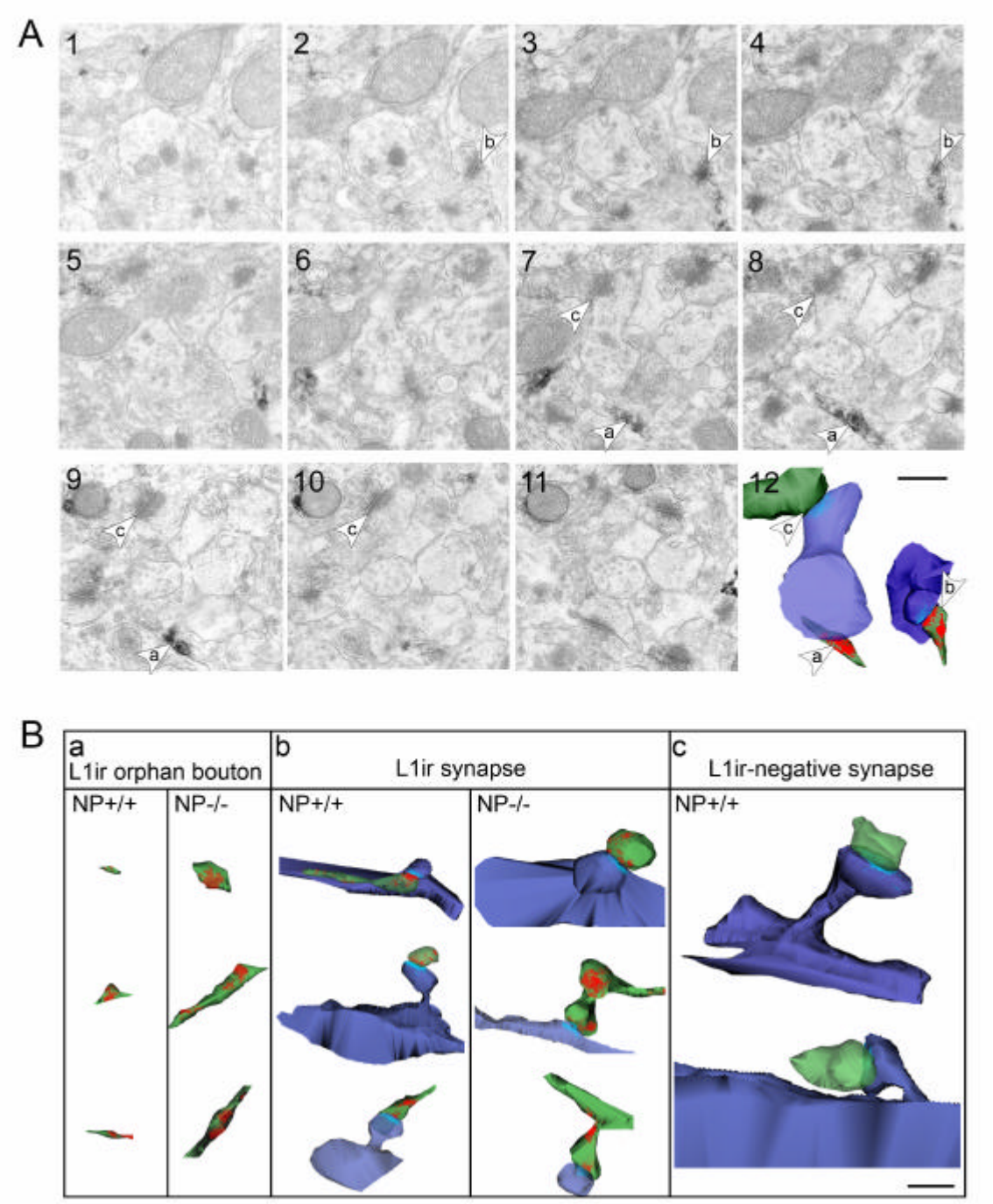

Figure 2. Morphology of L1ir and L1ir-negative synapses.

(A) Electron micrographs of consecutive ultrathin sections (1-11) and three-dimensional reconstruction demonstrating the L1ir orphan bouton (a), L1ir synapse (b) and L1ir-negative synapse (c) of the same microscopic field in NP+/+ mice (12).

(B) Complete three-dimensional reconstruction of L1ir orphan boutons (a), L1ir synapses (b) and L1ir-negative synapses (c) in NP+/+ and NP-/- mice. Reconstructed

presynapses are green, postsynapses are blue, their PSDs are light blue and L1-immunoreactive sites are red. Scale bar, 600 nm in all panels.

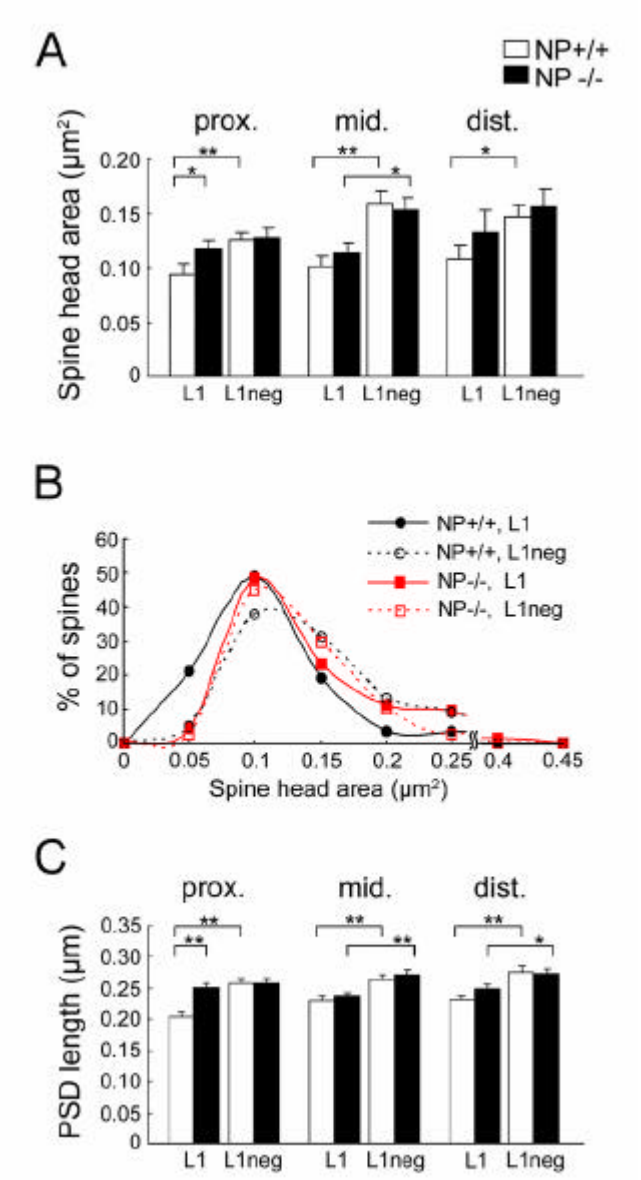

Figure 3. Shift from smaller to larger L1ir synapses in NP-/- mice.

(A) The stratum radiatum was divided into three regions, proximal (prox.), middle (mid.) and distal (dist.), according to distance from the CA1 soma. In NP+/+ mice (open bars), the mean cross-sectional spine head area of L1ir (L1) synapses is significantly smaller than that of L1ir-negative (L1neg) synapses in all regions of the stratum radiatum. The mean spine head area of L1ir synapses is larger in NP-/- mice (filled bars) than in NP+/+ mice (open bars), especially in the proximal region. *$p < 0.05$; **$p < 0.001$.

(B) The distribution of spine head area in the proximal region of L1ir synapses and L1ir-negative synapses in NP+/+ and NP-/- mice. In NP+/+ mice, L1ir synapses were

significantly smaller than L1ir-negative synapses (Kolmogorov-Smirnov test, $p < 0.03$). In NP-/- mice, the distribution of L1ir synapses shifted to a larger size, comparable to that of L1ir-negative synapses.

(C) The mean cross-sectional PSD length of L1ir synapses was significantly smaller than that of L1ir-negative synapses in NP+/+ (open) and NP-/- (closed) mice, except in the proximal region where the length of L1ir synapses in NP-/- mice was significantly larger than that in NP+/+ mice and comparable to the level in L1ir-negative synapses ($p>0.55$). *$p < 0.05$; **$p < 0.001$.

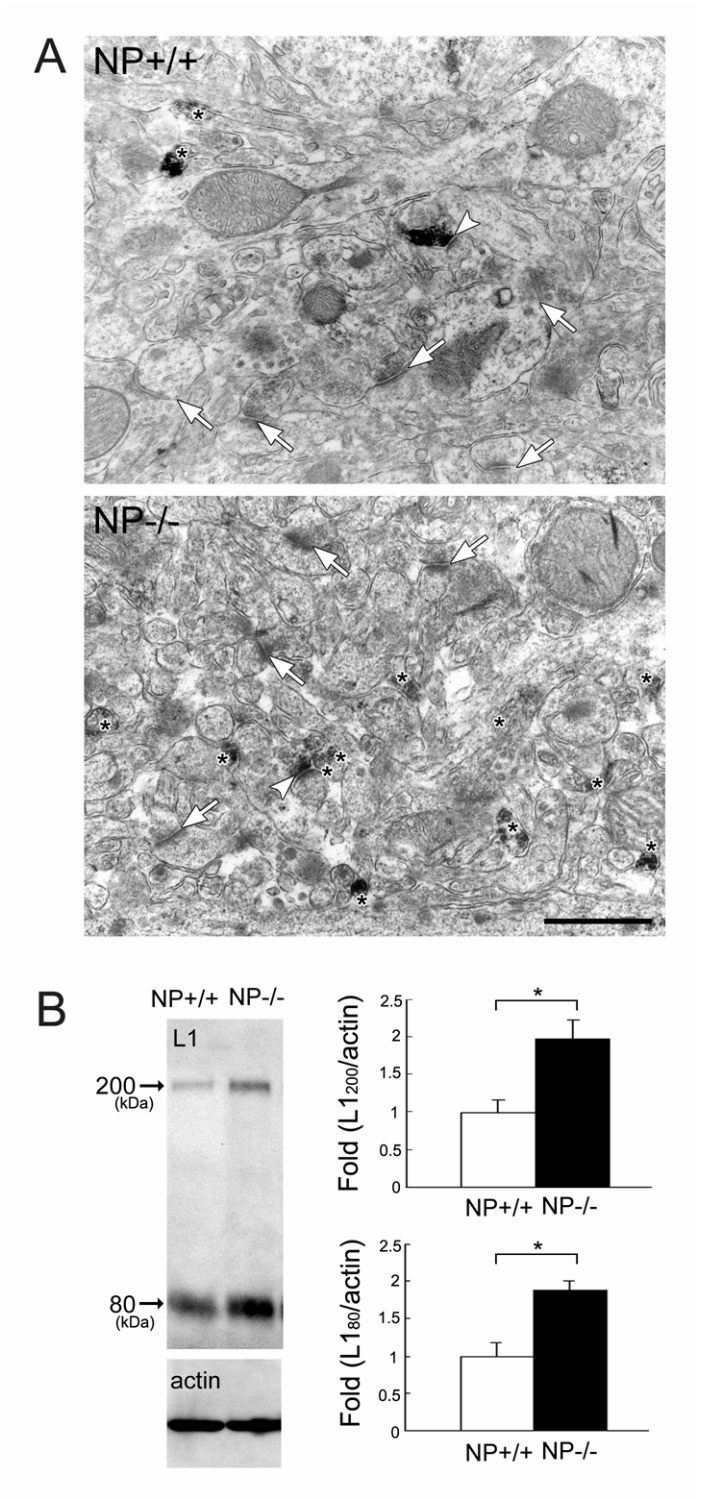

Figure 4. Change in the distribution of L1ir sites in NP-/- mice.

(A) Low-power immunoelectron micrographs of the proximal region of the CA1 stratum radiatum in NP+/+ (upper panel) and NP-/- (lower panel) mice. There are more

L1ir synaptic (arrowheads) and L1ir orphan boutons (asterisks) in the NP-/- mice than in the NP+/+ mice. Arrows show L1ir-negative synapses. Scale bar, 1 μm.
(B) Western blot analysis of L1 in hippocampus of NP+/+ and NP-/- mice. Both the 80 and 200 kDa L1ir bands were detectable. Actin served as internal control for protein loading. The graph shows the quantification of band intensities of $L1_{200}$ and $L1_{80}$. The band density of L1 was significant increase in NP-/- mice. $*p < 0.01$.

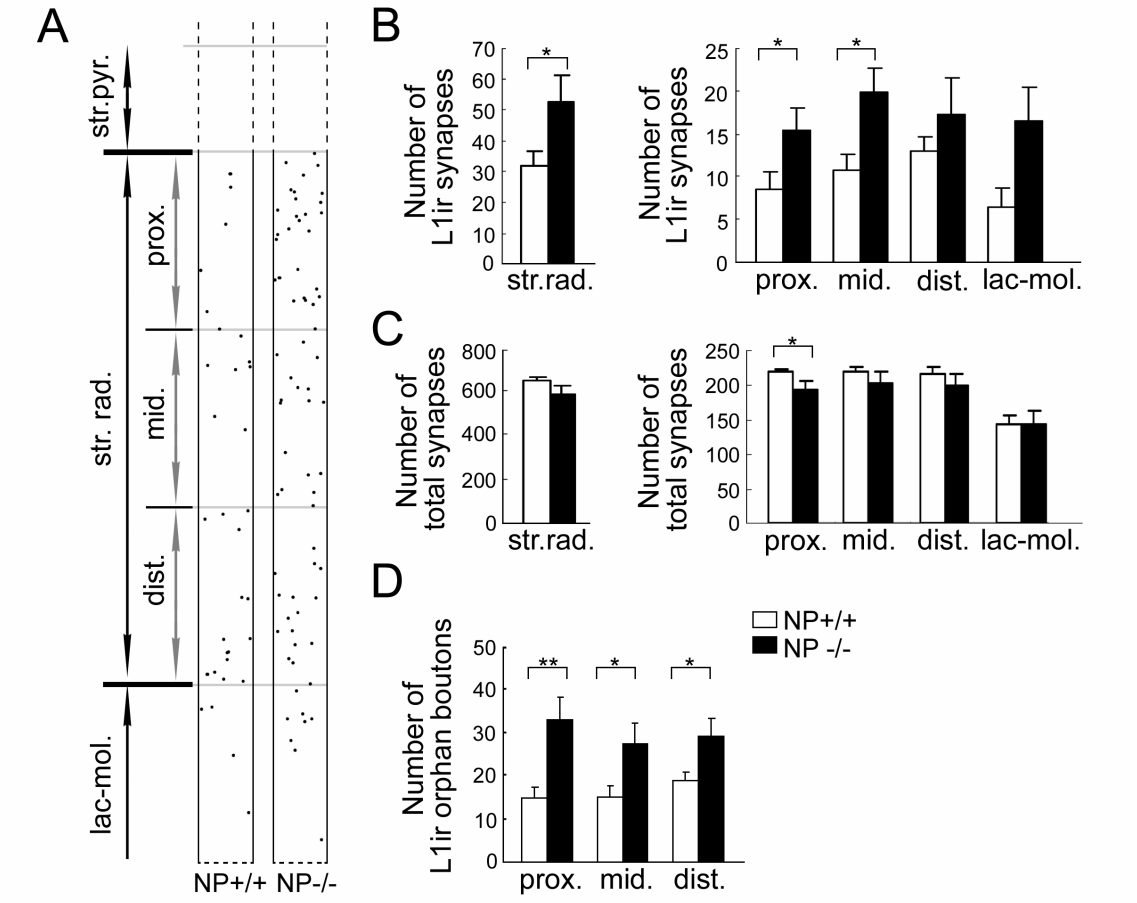

Figure 5. Increased number of L1ir synaptic and orphan boutons in NP-/- mice. (A) Typical distribution of L1ir synapses (dots) in NP+/+ (left) and NP-/- (right) mice in the CA1 subfield. L1ir synaptic boutons are plotted on a montage of 25 low-power (× 6000) electron micrographs of stratum pyramidale (str.pyr.), stratum radiatum (str.rad.) and stratum lacunosum moleculare (lac-mol.). The stratum radiatum (str. rad.) was divided into three regions, proximal (prox.), middle (mid.) and distal (dist.), according to the distance from CA1 soma.

(B) The number of asymmetrical L1ir synapses was counted in NP+/+ (open bars) and NP-/- (closed bars) mice. The left graph shows the number of L1ir synapses in a fixed area (13.0 × 219.6 μm) of the CA1 stratum radiatum, and the right graph shows the number in each region according to the distance from CA1 soma in a fixed area (13.0 × 73.2 μm). The mean number of L1ir synapses was significantly higher in NP-/- mice. *$p < 0.05$.

(C) Total number of asymmetrical synapses containing L1ir and L1ir-negative synapses

was counted in NP+/+ (open bars) and NP-/- (closed bars) mice. The left graph shows the number of synapses in the stratum radiatum in a fixed area (13.0 × 219.6 μm), and the right shows the number in each region depending on the distance from the CA1 soma in a fixed area (13.0 × 73.2 μm). The mean number of total synapses was significantly lower in the proximal region of NP-/- mice. *$p < 0.05$.

(D) The mean number of L1ir orphan boutons was significantly higher in NP-/- (closed bars) mice than NP+/+ (open bars) mice in the proximal region in a fixed area (13.0 × 16.5 μm). *$p < 0.05$; **$p < 0.01$.

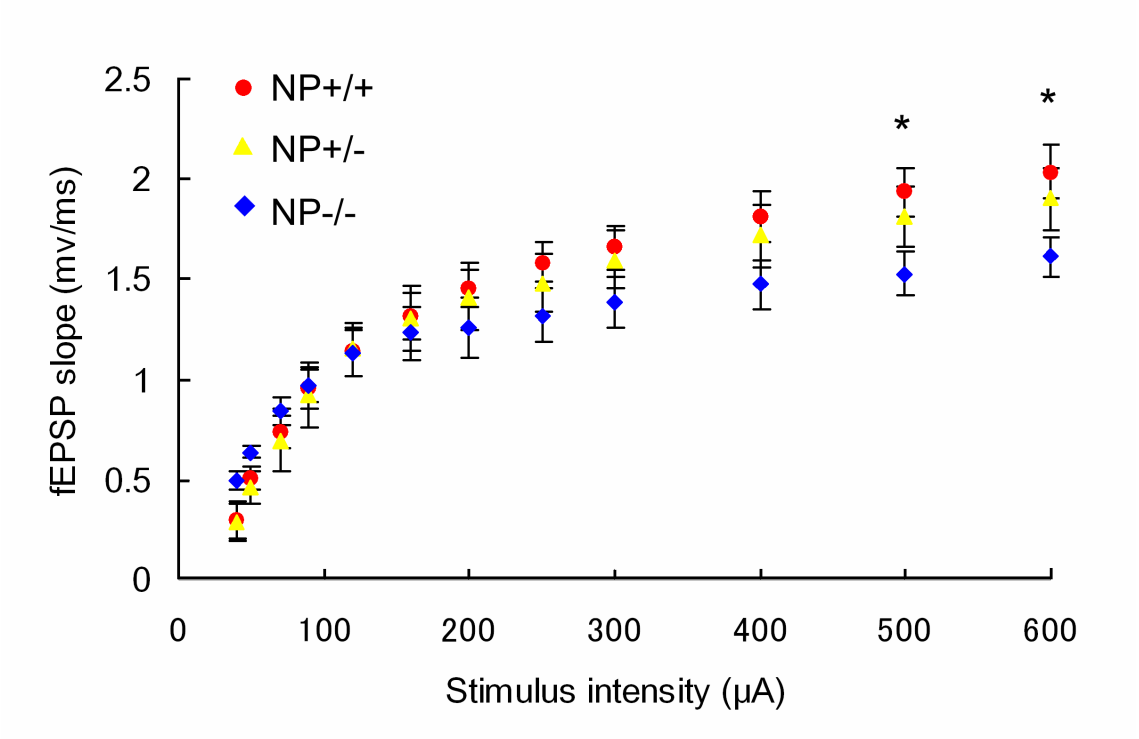

Figure 6 Input-output curves in NP+/+, NP+/-, NP-/- mice.

The mean evoked fEPSP across all mice is plotted as a function of stimulus strength for NP+/+ (●), NP+/- (▲) and NP-/- (◆) mice. There was a significant decrease between NP-/- and NP+/+ mice at stimulation intensities of 500 and 600 μA. Asterisks represent statistical signification between NP+/+ and NP-/- mice. *$p < 0.05$.

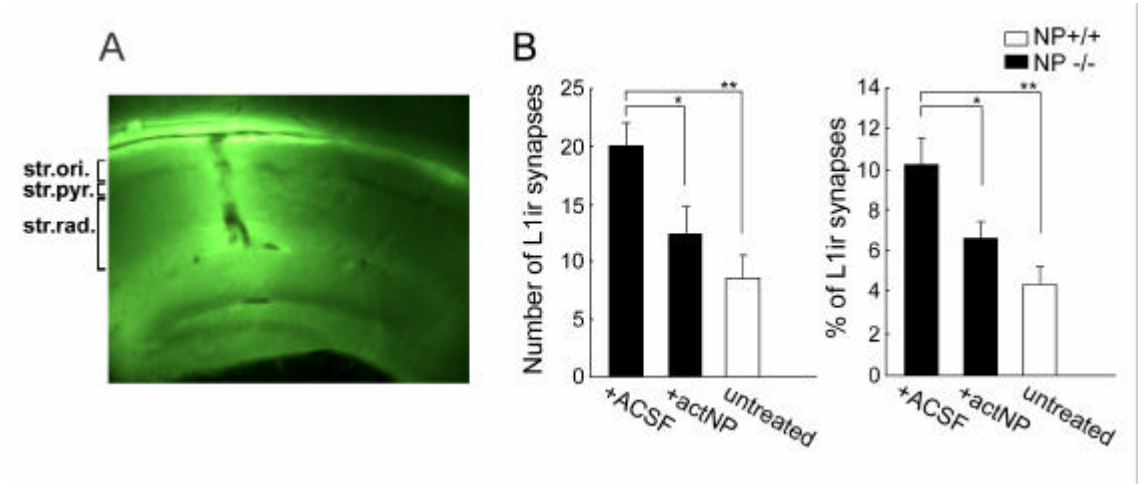

Figure 7. Injection of recombinant active NP into NP-/- mice restores L1ir synapses to NP+/+ levels.

(A) Fluorescent microscopic photograph represent spread of recombinant actNP in the hippocampus. Injection of FITC-conjugated recombinant actNP reaches the observation site of the stratum radiatum.

(B) Number (left) and percentage (right) of L1ir synapses one day after injection of ACSF or active NP (act NP) into NP-/- mice. The number and percentage of L1ir synapses were significantly decreased (actNP, closed bars; $*p < 0.05$) to the levels in untreated wild-type mice (untreated, open bars). There was no significant difference between the treated NP-/- mice and untreated wild-type mice (number, $p > 0.24$: percentage, $p > 0.08$). $**p < 0.001$.

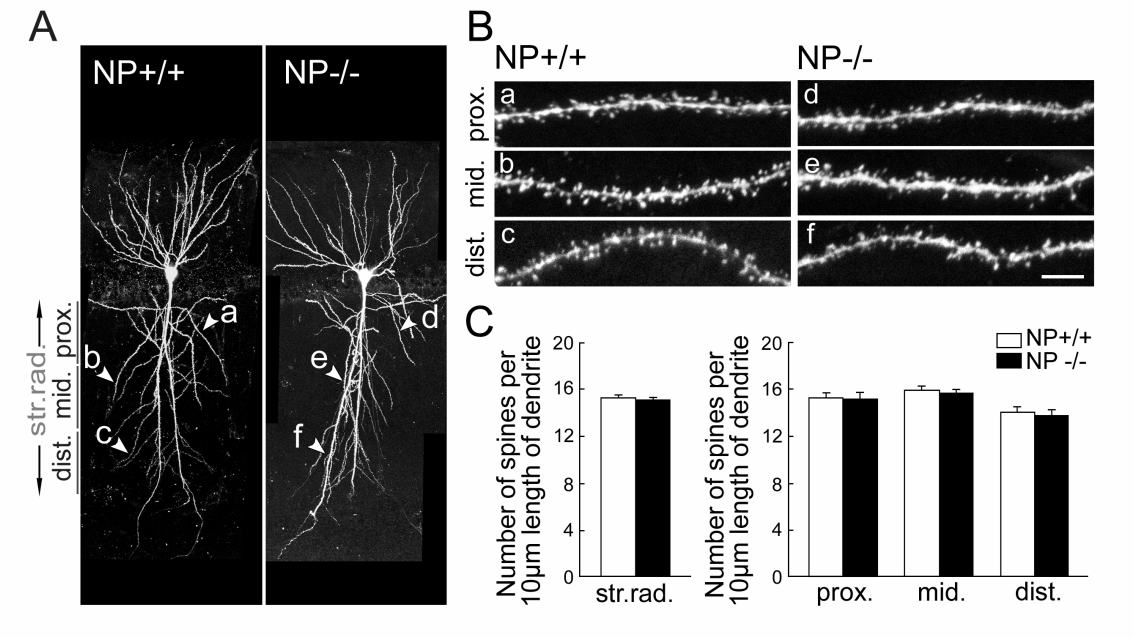

Figure 8. No difference in density of spines between NP+/+ and NP-/- mice.

(A) Fluorescence images of hippocampal CA1 pyramidal neurons of NP+/+ (left) and NP-/- mice (right) after injection of Lucifer Yellow. Arrowheads denote enlarged in B regions: proximal (prox.) (a and d), middle (mid.) (b and e) and distal (dist.) (c and f).

(B) Spine morphology of NP+/+ (left) and NP-/- (right) mice in prox. (a and d), mid. (b and e) and dist. (c and f) regions. Images are from the regions marked by the respective arrowheads in (A). Scale bar, 5 μm.

(C) Spines were counted in NP+/+ (open bars) and NP-/- (closed bars) mice. The left graph shows the density of spines in the stratum radiatum, and the right graph shows that in each region according to the distance from the CA1 soma. There was no difference in the density of spines between NP+/+ and NP-/- mice.

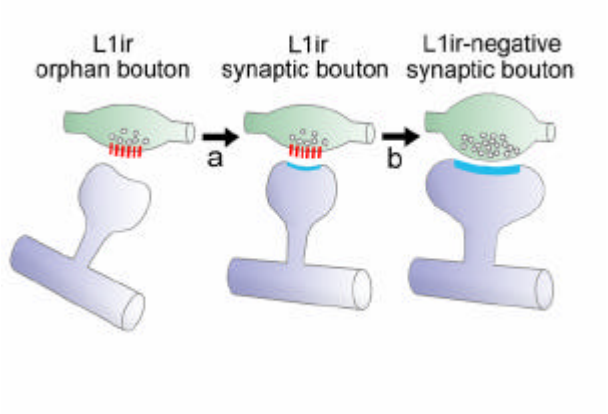

Figure 9. Diagrammatic model of synapse conversion.

Formation of synapses is divided into two phases, an early phase where L1ir orphan boutons make contact with small spines (a) and a late phase where small synapses containing L1 grow into large synapses lacking L1 (b). NP is considered to be involved in both phases. Presynaptic boutons are shown in pale green, spines in pale blue, PSD is bright blue, L1 in red, and synaptic vesicles as circles.

Table 1

Number and percentage of L1ir orphan and synaptic boutons in the stratum radiatum of NP-/- and NP+/+ mice

Orphan boutons

		Proximal		Middle		Distal		n
		Number	%	Number	%	Number	%	
	L1ir	70.5 ±11.5	(83.4 ±5.2)	62.6 ±10.6	(64.6 ±4.6)	83.8 ±10.8	(71.2 ±3.3)	8
NP+/+	L1ir-neg	11.5 ±3.1	(16.6 ±5.2)	31.3 ±5.0	(35.4 ±4.6)	32.5 ±4.7	(28.8 ±3.3)	8
	total	82.1 ±10.7		93.9 ±11.3		116.3 ±12.2		8
	L1ir	142.6 ±28.8*	(83.7 ±3.4)	134.2 ±28.9*	(74.4 ±4.6)*	145.9 ±24.3*	(83.9 ±2.5)**	8
NP-/-	L1ir-neg	19.2 ±2.0	(16.3 ±3.4)	28.9 ±3.8	(25.6 ±4.6)*	24.0 ±2.6	(16.1 ±2.5)**	8
	total	161.8 ±28.8*		163.0 ±35.8*		169.9 ±24.9		8

Synaptic boutons

		Proximal		Middle		Distal		
		Number	%	Number	%	Number	%	n
	L1ir	9.0 ±2.1	(3.8 ±0.9)	11.3 ±2.0	(4.9 ±0.8)	13.7 ±1.9	(6.1 ±0.9)	7
NP+/+	L1ir-neg	223.1 ±3.8	(96.2 ±0.9)	219.7 ±8.4	(95.1 ±0.8)	214.6 ±11.4	(93.9 ±0.9)	7
	total	232.1 ±4.3		231.1 ±8.8		228.3 ±11.6		7
	L1ir	16.4 ±2.7*	(8.1 ±1.2)**	21.0 ±2.6*	(10.4 ±1.8)**	18.2 ±4.5	(9.2 ±2.7)	7
NP-/-	L1ir-neg	188.4 ±12.2**	(91.9 ±1.2)**	191.9 ±17.7	(89.6 ±1.8)**	191.0 ±18.3	(90.8 ±2.7)	7
	total	204.8 ±12.8*		212.9 ±17.0		209.1 ±17.5		7

The numbers of boutons per 1000 μm^2 in proximal, middle and distal regions from the CA1 soma were counted (average ± SEM) and the percentages of L1ir and L1ir-negative (L1ir-neg) synaptic and orphan boutons per total (L1ir and L1ir-neg) are shown. Significant changes in the number and percentage of L1ir synaptic and orphan boutons between NP-/- and NP+/+ mice (Student's unpaired *t*-test) are indicated. *$p < 0.05$; **$p < 0.01$.

Discussion

L1 is known as a major adhesion molecule of growth cones, involved in elongation, fasciculation and pathfinding (Schachner, 1989; Burden-Gulley et al., 1995). However, its roles in mature synaptic functions such as synaptic plasticity are poorly understood. Previous immunohistochemical studies failed to observe L1ir in synapses of adult mice (Persohn and Schachner, 1990), although antibodies to L1 and a recombinant L1 fragment efficiently inhibited mature synaptic functions such as LTP (Luthi et al., 1994). In more recent (Matsumoto-Miyai et al., 2003; Munakata et al., 2003) and the present studies, I found L1-immunoreactivity in presynaptic immature boutons in the mature hippocampus, probably due to a thorough examination of all the layers of the stratum radiatum and the use of two kinds of L1-specific antibodies which appear to have minimum steric interference between the epitopic intracellular domain and other molecules. Additionally, close association of L1 with the presynaptic membrane could be observed using colloidal gold as an immunoreaction marker.

Recently, several investigators have described orphan boutons as another functioning synapse-like structure (Shepherd and Harris, 1998; Krueger et al., 2003). Krueger et al. (2003) revealed the presence of many orphan vesicle-release sites lacking postsynaptic specialization in cultured hippocampal neurons, and argued that they are

initiation sites of synaptogenesis. On the other hand, the size of the spine and PSD correlated directly with the amount of AMPA receptor (Harris and Stevens, 1989; Isaac et al., 1995; Liao et al., 1995; Schikorski and Stevens, 1999; Takumi et al., 1999), while a thin spine is thought to be an immature type of synapse that occurs during conversion to the mature mushroom spine (Tashiro and Yuste, 2004). Another report showed that dendritic spines are inducible by an extracellular factor at the cell surface as part of a receptor-ligand interaction (Passafaro et al., 2003). Thus, synaptogenesis may start at the onset of communication between orphan boutons and immature spines, followed by the maturation of synapse. Synapse formation may therefore be divided into two phases, as shown schematically in Fig. 9: an early phase where orphan boutons make contact with small spines (Fig. 9a), and a late phase where small synapses grow into large synapses (Fig. 9b). Between the early and the late phase, a high-frequency stimulus that elicits LTP may induce an NMDA receptor-dependent signaling cascade; these steps are involved in formation of memory, as shown by a number of studies (for a review, see Collingridge and Bliss (1995)).

In this study, I found orphan boutons in the CA1 stratum radiatum, and surprisingly, a considerable percentage of them (64-84%) were L1ir. On the other hand, most synaptic boutons were L1ir-negative (Table 1); in addition, the number of L1ir

synaptic vesicles was low and the morphology and size of spines contacted with L1ir boutons were thin and small. These data strongly suggest that L1 becomes localized at the beginning, of or immediately after, synaptogenesis, and that L1ir presynaptic boutons (including orphan boutons) are an immature type of transmission machinery. In NP-deficient mice, both L1ir orphan and synaptic boutons were observed in larger numbers, although the total number of synapses was decreased. The data suggest that maturation of synaptic structure was inhibited by NP deficiency. Since NP deficiency caused an accumulation of L1ir orphan and synaptic boutons, NP is likely to be involved in both phases; formation (a) and maturation (b) synapses (Fig. 9). This NP-related synaptogenesis/maturation may be important for neural plasticity, including learning and memory, because our previous data have shown that chemically induced LTP causes a brief rise in NP activity and breakdown of the L1 molecule in an NMDA receptor-dependent manner (Matsumoto-Miyai et al., 2003). Thus, both high-frequency stimuli and activation of NP may be required for NP-dependent synaptogenesis/maturation of L1ir boutons.

In the present study, I found that L1ir boutons accumulated and the total number of synapses decreased in NP-/- mice. The basal synaptic transmission of Schaffer-collateral CA1 synapses appears to be reduced in NP-/- mice (fig. 6), implying

that functional synapses decrease in the NP-/- hippocampus. Electrophysiological and quantitative immunoEM studies both indicated that mature and functional synapses decrease in the mutant, and therefore NP may mediate the conversion of immature synapses to mature synapses. The rather late expression of hippocampal NP mRNA during ontogeny indicates that NP has a major function in the adult stage (Suzuki et al., 1995). As shown by the experiment in which recombinant actNP was microinjected into NP-deficient mice (Fig. 7), NP retained the ability to convert boutons to the mature type. When actNP was injected into the CA1 region of the mature hippocampus of 8-week-old NP-/- mice, the number of L1ir synaptic boutons recovered to the level seen in the wild-type. Thus, conversion of L1ir synaptic boutons to L1ir-negative synapses may occur continuously in the adult hippocampus, presumably driven by an NMDA-dependent transient activation of proNP (Matsumoto-Miyai et al., 2003). In the NP-deficient mouse hippocampus, hypertrophied L1ir orphan and synaptic boutons were often observed. This may be caused by the continuous growth of synapses, without modification or stabilization of L1ir immature synapses by NP. Activity-dependent synaptic conversion from immature to mature by NP may trigger a chain reaction of a variety of LTP-related molecular events, such as the insertion of AMPA receptors, and molecular changes in adhesion molecules.

In this study, negative effects of NP deficiency were observed particularly in the proximal region from CA1 soma, although every layer in the stratum radiatum showed the same tendency. It has been shown recently that synaptic character varies according to distance from the soma, to differences in the distribution pattern of spines and A-type K^+ channels, and to synaptic responsiveness (Hoffman et al., 1997; Megias et al., 2001; Oray et al., 2004). Our present data and these earlier observations indicate that synaptic character is not homogeneous over the stratum radiatum, and that NP may be involved in activity-dependent synaptogenesis/maturation, most effectively in the proximal one-third of the stratum radiatum.

References

Benson, D. L., Schnapp, L. M., Shapiro, L. and Huntley, G. W. (2000). Making memories stick: cell-adhesion molecules in synaptic plasticity. *Trends Cell Biol* **10**, 473-82.

Burden-Gulley, S. M., Payne, H. R. and Lemmon, V. (1995). Growth cones are actively influenced by substrate-bound adhesion molecules. *J Neurosci* **15**, 4370-81.

Collingridge, G. L. and Bliss, T. V. (1995). Memories of NMDA receptors and LTP. *Trends Neurosci* **18**, 54-6.

Fiala, J. C. and Harris, K. M. (1999). Dendritic structure. In *Dendrite*, (eds G. Stuart N. Spruston and Hausser), pp. 1-34. New York: Oxford.

Franklin, K. B. J. and Paxinos, G. (1996). The mouse brain. San Diego: Academic press.

Harris, K. M. and Stevens, J. K. (1989). Dendritic spines of CA 1 pyramidal cells in the rat hippocampus: serial electron microscopy with reference to their biophysical characteristics. *J Neurosci* **9**, 2982-97.

Hirata, A., Yoshida, S., Inoue, N., Matsumoto-Miyai, K., Ninomiya, A., Taniguchi, M., Matsuyama, T., Kato, K., Iizasa, H., Kataoka, Y. et al. (2001). Abnormalities of synapses and neurons in the hippocampus of neuropsin-deficient mice.

Mol Cell Neurosci **17**, 600-10.

Hoffman, D. A., Magee, J. C., Colbert, C. M. and Johnston, D. (1997). K+ channel regulation of signal propagation in dendrites of hippocampal pyramidal neurons. *Nature* **387**, 869-75.

Horinouchi, K., Nakamura, Y., Yamanaka, H., Watabe, T. and Shiosaka, S. (2005). Distribution of L1-cam mRNA in the adult mouse brain: in situ hybridization and northern blot analyses. *J Comp Neurol* **482**, 386-404.

Isaac, J. T., Nicoll, R. A. and Malenka, R. C. (1995). Evidence for silent synapses: implications for the expression of LTP. *Neuron* **15**, 427-34.

Komai, S., Matsuyama, T., Matsumoto, K., Kato, K., Kobayashi, M., Imamura, K., Yoshida, S., Ugawa, S. and Shiosaka, S. (2000). Neuropsin regulates an early phase of schaffer-collateral long-term potentiation in the murine hippocampus. *Eur J Neurosci* **12**, 1479-86.

Krueger, S. R., Kolar, A. and Fitzsimonds, R. M. (2003). The presynaptic release apparatus is functional in the absence of dendritic contact and highly mobile within isolated axons. *Neuron* **40**, 945-57.

Liao, D., Hessler, N. A. and Malinow, R. (1995). Activation of postsynaptically silent synapses during pairing-induced LTP in CA1 region of

hippocampal slice. *Nature* **375**, 400-4.

Luthi, A., Laurent, J. P., Figurov, A., Muller, D. and Schachner, M. (1994). Hippocampal long-term potentiation and neural cell adhesion molecules L1 and NCAM. *Nature* **372**, 777-9.

Matsumoto-Miyai, K., Ninomiya, A., Yamasaki, H., Tamura, H., Nakamura, Y. and Shiosaka, S. (2003). NMDA-dependent proteolysis of presynaptic adhesion molecule L1 in the hippocampus by neuropsin. *J Neurosci* **23**, 7727-36.

Matsuzaki, M., Honkura, N., Ellis-Davies, G. C. and Kasai, H. (2004). Structural basis of long-term potentiation in single dendritic spines. *Nature* **429**, 761-6.

Megias, M., Emri, Z., Freund, T. F. and Gulyas, A. I. (2001). Total number and distribution of inhibitory and excitatory synapses on hippocampal CA1 pyramidal cells. *Neuroscience* **102**, 527-40.

Momota, Y., Yoshida, S., Ito, J., Shibata, M., Kato, K., Sakurai, K., Matsumoto, K. and Shiosaka, S. (1998). Blockade of neuropsin, a serine protease, ameliorates kindling epilepsy. *Eur J Neurosci* **10**, 760-4.

Munakata, H., Nakamura, Y., Matsumoto-Miyai, K., Itoh, K., Yamasaki, H. and Shiosaka, S. (2003). Distribution and densitometry mapping of L1-CAM Immunoreactivity in the adult mouse brain - light microscopic observation. *BMC*

Neurosci **4**, 7.

Oka, T., Hakoshima, T., Itakura, M., Yamamori, S., Takahashi, M., Hashimoto, Y., Shiosaka, S. and Kato, K. (2002). Role of loop structures of neuropsin in the activity of serine protease and regulated secretion. *J Biol Chem* **277**, 14724-30.

Okabe, A., Momota, Y., Yoshida, S., Hirata, A., Ito, J., Nishino, H. and Shiosaka, S. (1996). Kindling induces neuropsin mRNA in the mouse brain. *Brain Res* **728**, 116-20.

Oray, S., Majewska, A. and Sur, M. (2004). Dendritic spine dynamics are regulated by monocular deprivation and extracellular matrix degradation. *Neuron* **44**, 1021-30.

Passafaro, M., Nakagawa, T., Sala, C. and Sheng, M. (2003). Induction of dendritic spines by an extracellular domain of AMPA receptor subunit GluR2. *Nature* **424**, 677-81.

Persohn, E. and Schachner, M. (1990). Immunohistological localization of the neural adhesion molecules L1 and N-CAM in the developing hippocampus of the mouse. *J Neurocytol* **19**, 807-19.

Schachner, M. (1989). Families of neural adhesion molecules. *Ciba Found Symp* **145**, 156-69, discussion 169-72.

Schikorski, T. and Stevens, C. F. (1999). Quantitative fine-structural analysis of olfactory cortical synapses. *Proc Natl Acad Sci U S A* **96**, 4107-12.

Shepherd, G. M. and Harris, K. M. (1998). Three-dimensional structure and composition of CA3-->CA1 axons in rat hippocampal slices: implications for presynaptic connectivity and compartmentalization. *J Neurosci* **18**, 8300-10.

Shimizu, C., Yoshida, S., Shibata, M., Kato, K., Momota, Y., Matsumoto, K., Shiosaka, T., Midorikawa, R., Kamachi, T., Kawabe, A. et al. (1998). Characterization of recombinant and brain neuropsin, a plasticity- related serine protease. *J Biol Chem* **273**, 11189-96.

Shiosaka, S. and Yoshida, S. (2000). Synaptic microenvironments--structural plasticity, adhesion molecules, proteases and their inhibitors. *Neurosci Res* **37**, 85-9.

Suzuki, J., Yoshida, S., Chen, Z. L., Momota, Y., Kato, K., Hirata, A. and Shiosaka, S. (1995). Ontogeny of neuropsin mRNA expression in the mouse brain. *Neurosci Res* **23**, 345-51.

Takumi, Y., Ramirez-Leon, V., Laake, P., Rinvik, E. and Ottersen, O. P. (1999). Different modes of expression of AMPA and NMDA receptors in hippocampal synapses. *Nat Neurosci* **2**, 618-24.

Tashiro, A. and Yuste, R. (2004). Regulation of dendritic spine motility and

stability by Rac1 and Rho kinase: evidence for two forms of spine motility. *Mol Cell Neurosci* **26**, 429-40.

Acknowledgments

I would like to express my sincerest gratitude toward Drs. Sadao Shiosaka, Kazunori Imaizumi, Keiko Kato, Kazumasa Matsumoto-Miyai, Yasuyuki Ishikawa, Shoji Komai and all members of division of structural cell biology in Nara Institute of Science and Technology (NAIST).

I thank Dr. Vance Lemmon of University of Miami School of Medicine and Prof. Ian R.L. Smith of Nara Institute of Science and Technology.

I also thank Dr. Yoshinori Kawai of The Jikei University School of Medicine and Dr. Megumi Iwano and Satuki Takahasi of Nara Institute of Science and Technology for useful advices on electronmicroscopic technique.

This work is supported in part by a Grant-in-Aid for 21st Century COE Research from Ministry of Education, Culture, Sports, Science and Technology.

I wish to dedicate this thesis to all members of my family, whose love and encouragement have supported me throughout my training.